THE ASTRONOMICAL JOURNAL, 121:1369–1384, 2001 March

THE NONSTELLAR INFRARED CONTINUUM OF SEYFERT GALAXIES[1]

ALMUDENA ALONSO-HERRERO[2] AND ALICE C. QUILLEN
Steward Observatory, 933 North Cherry Avenue, University of Arizona, Tucson, AZ 85721
CHRIS SIMPSON
Subaru Telescope, National Astronomical Observatory of Japan, 650 North A'Ohōkū Place, Hilo, HI 96720
ANDREAS EFSTATHIOU
Astrophysics Group, Imperial College London, Blackett Laboratory, Prince Consort Road, London SW7 2BZ, England, UK
AND
MARTIN J. WARD
Department of Physics and Astronomy, University of Leicester, Leicester LE1 7RH, England, UK
Received 2000 October 16; accepted 2000 November 17

ABSTRACT

JHKL'M (1–5 μm) imaging of a sample of Seyfert 2 galaxies is presented. We have performed an accurate estimate of the near-infrared nonstellar nuclear fluxes. We confirm that the near-infrared nuclear continuum between 1 and 2.2 μm of some Seyfert 2s is dominated by stellar emission, whereas the continuum emission at longer wavelengths ($\lambda = 3$–5 μm) is almost entirely nonstellar in origin. The nonstellar spectral energy distributions (SED) in the infrared (up to 15 μm) of Seyfert galaxies show a variety of shapes, and they are well reproduced with the tapered disk models of Efstathiou & Rowan-Robinson. We have used two models, one including an optically thin cone component found to fit the SED of NGC 1068 and a coneless model. Although our modeling of the SEDs does not allow us to favor either model to account for all the observed SEDs, we find that the viewing angle toward the central source is well constrained by both models. The galaxies in our sample have fitted values of the viewing angle in the range $\theta_v = 0°$–$64°$, for the assumed model parameters. We have also investigated nonstellar color-color diagrams ($L'-M$ vs. $H-M$ and $L'-M$ vs. $H-L'$). The colors of the Seyfert galaxies with viewing angles $\theta_v < 30°$ are better reproduced with the cone model. These diagrams provide a good means to separate Seyfert 2s with moderate obscuration ($A_V \lesssim 20$ mag from hard X-ray observations) from those with high obscuration.

The ground-based 4.8 μm and ISO 9.6 μm luminosities are well correlated with the hard X-ray luminosities of Seyfert 1s and 2s. These continuum emissions appear as a good indicator of the AGN luminosity, at least in the cases of hard X-ray Compton-thin Seyfert galaxies ($N_{\rm H} \leq 10^{24}$ cm^{-2}). We finally stress the finding that some Compton thick galaxies show bright nonstellar emission at 5 μm. This suggests that the near-infrared emission in Seyfert galaxies is produced in an extended component illuminated by the central source, that is more visible from all viewing angles, providing a good explanation for the differing $N_{\rm H}/A_V$ ratios found in some Seyfert 2s. We discuss possible implications of mid-infrared surveys for the search of counterparts of highly obscured hard X-ray sources.

Key words: galaxies: active — galaxies: nuclei — galaxies: photometry — galaxies: Seyfert — galaxies: stellar content — infrared: galaxies

1. INTRODUCTION

There is now considerable evidence that the infrared emission in active galaxies (Seyfert galaxies and radio quiet quasars) is thermal in origin, namely hot dust emission (e.g., Rieke & Low 1975; Rieke 1978; Barvainis 1987; McAlary & Rieke 1988; Sanders et al. 1989; Danese et al. 1992; and recently Andreani, Franceschini, & Granato 1999; Haas et al. 2000; Polletta et al. 2000, and references therein). The strong mid- and far-infrared emission in active galactic nuclei is often interpreted as produced by a disklike (Sanders et al. 1989) or torus-like (e.g., Pier & Krolik 1992; Granato & Danese 1994; Efstathiou & Rowan-Robinson 1995, among others) dust configuration heated by the central source. This obscuring material which hides a direct view of the central source in type 2 objects, absorbs a large fraction of the X-ray/UV/optical energy emitted by the central source and reradiates it in the infrared spectral range.

The nature of the nonstellar infrared continuum in Seyfert 2 galaxies, where the stellar component dominates the nuclear near-infrared emission (Edelson & Malkan 1986; Alonso-Herrero, Ward, & Kotilainen 1996), has eluded us because of the difficulty in estimating the nonstellar contribution at near-infrared wavelengths (up to 2 μm). High-resolution near-infrared images observed with NICMOS on the *HST* have now been used to detect and measure the nuclear nonstellar emission in Seyfert galaxies

[1] This work is based on observations collected at UKIRT. The UKIRT is operated by the Joint Astronomy Centre on behalf of the UK Particle Physics and Astronomy Research Council. Based on observations with the NASA/ESA *Hubble Space Telescope*, obtained at the Space Telescope Science Institute, which is operated by the Association of Universities for Research in Astronomy, Inc., under NASA contract NAS 5-26555.

[2] Current address: Department of Physical Sciences, University of Hertfordshire, College Lane, Hatfield, Herts, AL10 9AB, England, UK.

(Quillen et al. 2001a). This work reported that almost 100% of all Seyfert 1–1.9 galaxies and 50% of all Seyfert 2s show point sources at 1.6 μm. This unresolved emission is variable in some of the Seyfert 2s and thus is presumably nonstellar emission associated with the central engine (Quillen et al. 2000). The high detection rate of point sources in the near-infrared is in contrast with the small number of point sources reported in Seyfert 2s in the *HST* optical survey of Malkan, Gorjian, & Tam (1998). Previous attempts to model the nonstellar spectral energy distributions (SEDs) of Seyfert 2s (e.g., Edelson & Malkan 1986 and recently Fadda et al. 1998, and references therein) suffered from a number of problems, including large aperture photometry and uncertain determinations of the stellar component which may dominate the near-infrared emission up to 2.2 μm of Seyfert 2s. To date, a detailed modeling of SEDs has been restricted to individual galaxies (e.g., NGC 1068, Efstathiou, Hough, & Young 1995; NGC 3281, Simpson 1998; CenA, Alexander et al. 1999; the Circinus galaxy, Ruiz et al. 2001). An additional problem may exist when nonsimultaneous observations are used since some Seyfert 1.8s and 1.9s are now found to show variability at near-infrared wavelengths over timescales of several months (Quillen et al. 2000 from *HST*/NICMOS observations at 1.6 μm).

Models of dusty tori with different geometries (e.g., Pier & Krolik 1992; Granato & Danese 1994; Efstathiou & Rowan-Robinson 1995; Granato, Danese, & Franceschini 1997) predict bright infrared emission, making the *L*-band (at 3.5 μm) and *M*-band (at 4.8 μm) well suited to study the nature of the nonstellar emission in Seyfert galaxies. Because of the strong dependence of the infrared emission with the viewing angle and the geometry of the obscuring material, infrared SEDs can be used to constrain the torus parameters in Seyfert galaxies. An additional advantage is that the stellar contribution is greatly reduced longward of 2 μm, even for Seyfert 2s (Alonso-Herrero et al. 1996). The use of observations at longer wavelengths >50 μm (e.g., *IRAS* and *ISO* measurements), while useful in determining the bolometric emission, are problematic when trying to separate the contributions from the central AGN and a possible circumnuclear starburst, because of the large apertures employed.

In this paper we present near-infrared (from 1 to 5 μm) imaging observations of a small sample of Seyfert 1.9–2 galaxies which are complemented with *HST*/NICMOS and ISO imaging, covering a spectral range from 1 μm up to 15 μm. In a future paper (Quillen et al. 2001b) we will discuss the infrared properties and SEDs of the Seyfert 1.8–2s in the CfA sample. The paper is organized as follows, in § 2 we describe the observations, in § 3 we determine the nonstellar emission, and in § 4 we analyze the observed nonstellar energy distributions, nonstellar color-color diagrams and compare them with the outputs from torus models. In § 5 we will show that the 5–10 μm fluxes are a good indicator for the AGN luminosity for Compton-thin AGNs. Conclusions are presented in § 6.

2. OBSERVATIONS

2.1. *UKIRT Observations*

We obtained J ($\lambda_c = 1.25$ μm), H ($\lambda_c = 1.65$ μm), K ($\lambda_c = 2.20$ μm), L' ($\lambda_c = 3.80$ μm) and M ($\lambda_c = 4.80$ μm) imaging of a sample of 14 Seyfert 1.9 and Seyfert 2 galaxies (see Table 1) with the infrared camera IRCAM3 on the 3.9 m United Kingdom Infrared Telescope (UKIRT) during two observing runs in 1997 September and 1998 April. The size of the J, H, and K images is 256 × 256 pixels with pixel size of 0.″143 pixel^{-1}, whereas the size of the $L'M$ images is 64 × 64 pixels, with pixel size 0.″286 pixel^{-1}.

Standard reduction procedures were applied. Conditions were photometric during both runs, so standard star observations from the Elias et al. (1982) list (for $JHKL'$) and from the UKIRT list of photometric standards (for M) were used to perform the photometric calibration of the images. The major source of uncertainty in near-infrared observations comes from the background subtraction, especially at the longer wavelengths (L' and M). Typical errors from the photometric calibration are 0.09, 0.04, 0.08, 0.07, and 0.10 mag in J, H, K, L', and M, respectively. The FWHM seeing was measured from the standard stars 0.″6–0.″7 at K band for both runs.

Standard synthetic aperture photometry was performed on all the images using a 3″ diameter circular aperture (Table 2). The errors associated with the sky subtraction at

TABLE 1

LOG OF UKIRT AND *HST*/NICMOS OBSERVATIONS

Galaxy (1)	UKIRT (2)	Date (3)	NICMOS (4)	Date (5)	Var. (6)	Timescale (months) (7)
NGC 1052	*JHKL'M*	1997 Sep	NIC2 F160W	1998 Sep	...	...
NGC 1068	*JHKL'M*	1997 Sep	NIC2 F110W, F160W, F222M	1998 Feb	...	...
NGC 1097	*JHKL'M*	1997 Sep	...	...	...	...
NGC 2992	*JHKL'M*	1998 Apr	NIC2 F205W	1998 Nov	...	...
NGC 4968	*JHKL'M*	1998 Apr	NIC2 F160W	1998 May	...	...
NGC 5252[a]	*M*	1998 Apr	NIC1 F110W, F160W	1998 Mar, 1998 Apr	No	1 month
NGC 5506	*JHKL'M*	1998 Apr	NIC2 F160W, F205W	1998 Apr, 1998 Aug	...	...
NGC 7172	*JHKL'M*	1997 Sep	...	...	...	...
NGC 7217	*JHKL'M*	1997 Sep	NIC1 F110W, F160W	1997 Aug	...	...
Mrk 1	*JHKL'*	1997 Sep	NIC1 F160W	1997 Sep	...	...
Mrk 348[a]	*M*	1997 Sep	...	...	...	...
Mrk 533	*JHKL'M*	1997 Sep	NIC1 F110W, F160W	1998 Sep, 1997 Sep	Yes	14
Mrk 573[a]	*M*	1997 Sep	NIC1 F110W, F160W	1998 Aug	No	12
MCG −5-23-16	*JHKL'M*	1998 Apr	...	...	...	...

[a] *JHKL'* imaging can be found in Alonso-Herrero et al. (1998).

TABLE 2

UKIRT PHOTOMETRY THROUGH A 3″ DIAMETER APERTURE FOR THE SEYFERT 2 SAMPLE

Galaxy	J	H	K	L'	M
NGC 1052	11.40	10.66	10.39	9.77 ± 0.02	9.08 ± 0.23
NGC 1068	10.42	9.08	7.54	4.53 ± 0.02	3.24 ± 0.02
NGC 1097[a]	11.95	10.99	10.75	10.19 ± 0.17	>10.50
NGC 2992	12.34	11.50	10.94	10.01 ± 0.10	9.15 ± 0.30
NGC 4968	13.26	12.39	11.61	9.98 ± 0.05	8.65 ± 0.20
NGC 5252[b]	13.27	12.56	12.03	10.58 ± 0.04	10.04 ± 0.30
NGC 5506	12.09	10.46	9.14	7.11 ± 0.03	6.22 ± 0.02
NGC 7172	12.74	11.76	10.91	9.50 ± 0.02	8.56 ± 0.05
NGC 7217[a]	11.99	11.27	10.96	10.88 ± 0.15	>10.60
Mrk 1	14.12	13.33	12.89	11.26 ± 0.10	...
Mrk 348[b]	13.52	12.72	12.17	10.50 ± 0.04	9.06 ± 0.10
Mrk 533	13.38	12.28	11.21	9.14 ± 0.02	7.95 ± 0.08
Mrk 573[b]	12.87	12.27	11.78	10.14 ± 0.04	8.98 ± 0.30
MCG −5-23-16.....	11.94	11.01	10.22	8.51 ± 0.02	7.67 ± 0.06

[a] The M-band limits for NGC 1097 and NGC 7217 are 3 σ.

[b] $JHKL'$-band photometry from Alonso-Herrero et al. (1998). The quoted errors for the L'- and M-band photometry account only for the sky subtraction uncertainties, except for the Alonso-Herrero et al. (1998) L'-band photometry, which are only the photometric errors.

L and M are given together with the aperture photometry in the last two columns of Table 2.

2.2. *HST/NICMOS Observations*

We searched the *HST* archive for broadband NICMOS observations of our sample of galaxies. In Table 1 columns (4) and (5) we list the camera and filter, and the observation date, respectively. In columns (6) and (7) we indicate if variability has been found, and the timescale from Quillen et al. (2000). The plate scales for cameras NIC1 and NIC2 are 0.″045 pixel^{-1} and 0.″076 pixel^{-1}, respectively.

The images were reduced with routines from the package

TABLE 3

MID-INFRARED ISO FLUXES

Galaxy (1)	λ (μm) (2)	Flux (mJy) (3)	Reference (4)
NGC 1068.....	5.9	8660	Rigopoulou et al. (1999)
	7.7	14500	Rigopoulou et al. (1999)
NGC 3227.....	6.75	294, 249	Clavel et al. (2000)
	9.63	382, 372	Clavel et al. (2000)
	16	1220	Pérez García & Rodríguez Espinosa (2000)
NGC 3281.....	11.4	530	This work
NGC 4151.....	5.9	882	Rigopoulou et al. (1999)
	7.7	1090	Rigopoulou et al. (1999)
	16	4120	Pérez García & Rodríguez Espinosa (2000)
NGC 5252.....	6.75	14.8	Quillen et al. (2001b)
	9.63	27.1	Quillen et al. (2001b)
	11.4	34.6	Quillen et al. (2001b)
	15	44.8	Quillen et al. (2001b)
NGC 5506.....	5.9	646	Rigopoulou et al. (1999)
	7.7	713	Rigopoulou et al. (1999)
	11.4	890	This work
NGC 5548.....	6.75	170	Clavel et al. (2000)
	9.63	270	Clavel et al. (2000)
	16	440	Pérez García & Rodríguez Espinosa (2000)
NGC 7172.....	6.75	160	This work
	15	240	This work
NGC 7469.....	5.9	270	Rigopoulou et al. (1999)
	6.75	433	This work
	7.7	539	Rigopoulou et al. (1999)
	15	1290	This work
Mrk 1.....	5.9	20.9	Rigopoulou et al. (1999)
	7.7	88.3	Rigopoulou et al. (1999)
Mrk 348	6.75	65	This work
	15	270	This work
Mrk 533	6.75	259, 213	Clavel et al. (2000)
	9.63	345	Clavel et al. (2000)
IC 4329A	6.75	591, 477	Clavel et al. (2000)
	9.63	890, 739	Clavel et al. (2000)

NICRED (McLeod 1997). The main steps in the data reduction involve subtraction of the first readout, dark current subtraction on a readout-by-readout basis, correction for linearity and cosmic-ray rejection (using FULLFIT), and flat fielding. Darks with sample sequences and exposure times corresponding to those of our observations were obtained from other programs close in time to ours. Usually between 10 and 20 darks were averaged together (after the subtraction of the first readout) for a given sample sequence. Flat-field images were constructed from on-orbit data.

The photometric calibration of the NICMOS images was performed using the conversion factors based on measurements of the standard star P330-E (M. Rieke 1999, private communication). Comparisons of the ground-based H-band aperture photometry with the NICMOS F160W filter show that differences are always less than 15%, whereas the comparison of ground-based K-band photometry with that of the NICMOS F222M and F205W filters agrees within 25%.

2.3. *Comparison Sample of Seyfert 1s*

As a comparison sample, we also searched the *HST* archive for Seyfert 1–1.5 galaxies with 1–2.2 μm NICMOS observations, as well as with ground-based L (or L') and M small aperture photometry and *ISO* observations.

2.4. *ISO Observations*

We searched the literature for available mid-infrared *ISO* (from 5 μm up to 15 μm) continuum fluxes. In addition, for those galaxies with unpublished data, we obtained images from the ISO archive. The photometric calibration was that of the pipeline for which the typical errors are $\pm 15\%$. The *ISO* fluxes were measured using 12″ diameter apertures and aperture corrections measured from model PSFs. This procedure is very similar to that employed by Clavel et al (2000). NGC 5506 and NGC 7469 looked like point sources, so contamination by nearby star formation was not likely to be a large problem. For the brightest source (NGC 5506) some additional problems may be caused by saturating the detector. The wavelengths, fluxes, and references for the *ISO* data for the galaxies in our sample of Seyfert 2s and Seyfert 1s are given in Table 3.

3. DETERMINATION OF THE NONSTELLAR FLUXES

3.1. *The 1–2.2 μm Spectral Range*

As mentioned in the introduction it is essential to obtain very accurate estimates of the nonstellar emission to understand and model the SEDs of Seyfert 2s. The stellar component may dominate most of the nuclear flux for wavelengths up to 2 μm in Seyfert 2s (Alonso-Herrero et al. 1996). The relatively small field of view of the ground-based JHK (36″ × 36″) and NICMOS images (19″ × 19″ and 11″ × 11″ for NIC2 and NIC1 observations, respectively) prompted us to try a nucleus + bulge decomposition of the observed radial surface brightness profiles. We used a similar method to that employed in Alonso-Herrero et al. (1996). For the ground-based UKIRT observations the nuclear component was assumed to be a delta function convolved a Gaussian profile to account for the seeing effects (see Alonso-Herrero et al. 1996 for more details). For the NICMOS observations, the nuclear component was represented with a surface brightness profile of a point-spread function (PSF) generated with the TinyTim software (Krist et al. 1998). The bulge component was represented with a de Vaucouleurs $r^{1/4}$ profile. The surface brightness profiles were extracted out to radial distances of 5.″7, 4.″6, and 2.″6 for the ground-based data, NIC2, and NIC1 data, respectively.

We opted for a nucleus + bulge deconvolution instead of the method used in Simpson (1998). His method consisted in scaling an annulus of the J-band images to the observed counts in H and K, and then assuming that the nonstellar component makes no significant contribution to the J-band to estimate the nonstellar component in H and K. This method works so long as the nonstellar component in J is negligible. From our surface brightness profile deconvolution however, we find that in most cases although the nonstellar component at J is small, it is not negligible. Only in the case of Mrk 348, did we use Simpson's method for the H- and K-band images, because only lower angular resolution data (from Alonso-Herrero et al. 1998) were available. As done by Simpson (1998), we checked that the J-band nonstellar flux for Mrk 348 was negligible by extrapolating the stellar $HKL'M$ fluxes to the J-band and comparing with the observed flux.

After performing the nucleus + bulge deconvolution we measured the unresolved flux, which will be assumed to be nonstellar in origin, and its contribution within a 3″ diameter aperture. The nonstellar fractions within this aperture are given in columns (7), (8), and (9) for JHK, respectively, for the ground-based data, and in parenthesis for the NICMOS data when available. The nonstellar fraction within a 3″ aperture (which corresponds to projected angular sizes of between 200 pc and 1.5 kpc for our sample of galaxies) gives an estimate of the dominance or otherwise of the nonstellar component at a given wavelength. In Table 4, columns (2), (3), and (4) we give the JHK nonstellar fluxes using the NICMOS nonstellar fractions (when available) and the ground-based photometry. Note that we did not detect an unresolved component at 1–2.2 μm in NGC 1097 and NGC 7217, and therefore these two galaxies are excluded from the following analysis. We performed a similar analysis on the NICMOS images as with the Seyfert 2s to derive the nonstellar fluxes from 1 to 2.2 μm (see Table 5).

As discussed in Alonso-Herrero et al. (1996) the main source of uncertainty in the determination of the unresolved fluxes from the ground-based data is the fitted value to the seeing. Because of the relatively small field of view of the images, no stars are present in the images. However, the fitted values of the seeing from the profile deconvolution are very similar to the values of the FWHM measured from the standard stars observed close in time. On the other hand, the advantage of using NICMOS images is that the NIC1 and NIC2 PSF is very stable, is very well sampled and can be well modeled with the TinyTim software. Therefore the estimated nonstellar fluxes from NICMOS profiles are less affected by uncertainties. An upper limit to the errors associated with the nonstellar flux determination can be obtained by comparing the nonstellar fractions derived from the ground-based and the NICMOS images. The differences are never greater than 45%, and they tend to increase for shorter wavelengths where the nonstellar contributions are smaller.

Our estimates are in relatively good agreement (to within the uncertainties given above) for those galaxies in common

TABLE 4

NONSTELLAR FLUXES AND NONSTELLAR CONTRIBUTION WITHIN A 3″ DIAMETER APERTURE FOR THE SEYFERT 2 SAMPLE

Galaxy (1)	$f(J)$ (mJy) (2)	$f(H)$ (mJy) (3)	$f(K)$ (mJy) (4)	$f(L')$ (mJy) (5)	$f(M)$ (mJy) (6)	J (percent) (7)	H (percent) (8)	K (percent) (9)	L' (percent) (10)
NGC 1052	No	No	<0.9	<20.2	38.0	No	No (0)	<2	<65
NGC 1068	9.8	97.6	449.6	3690.8	8245.0	17 (9)	47 (41)	69 (71)	95
NGC 2992	No	<1	2.8	22.7	35.7	No	No	10 (23)	91
NGC 4968	No	0.6	3.7	23.2	56.5	No	5 (7)	25	90
NGC 5252	No	0.7	1.0	11.1	15.7	No	4 (7)	10	75
NGC 5506	13.8	59.0	120.4	340.1	530.0	59	79 (89)	64 (83)	95
NGC 7172	No	<0.4	3.4	30.0	61.4	No	<2	12	75
Mrk 1	<0.07	0.15	0.8	6.4	...	<2	3 (7)	18	80
Mrk 348	<1	0.6	2.7	14.5	38.7	<2	7	30	91
Mrk 533	1.0	5.0	12.3	53.0	108.6	23 (14)	31 (40)	57	95
Mrk 573	0.2	0.6	3.2	18.8	41.3	(2)	(6)	25	85
MCG −5-23-16.....	1.1	3.7	10.7	79.5	139.4	4	9	20	80

NOTE.—The zero points used for $JHKL'M$ are: 1600, 1020, 657, 252, and 163 Jy, respectively. The 3″ diameter M-band fluxes are assumed to be all nonstellar. "No" means that no unresolved component was detected.

with Zitelli et al. (1993), Kotilainen et al. (1992), Alonso-Herrero et al. (1996), and Quillen et al. (2001a, 2001b). We confirm the findings of Alonso-Herrero et al. (1996), that the 1 to 2.2 μm continuum of some Seyfert 2 galaxies is dominated by stellar emission. However, the stellar contribution decreases significantly at longer wavelengths.

3.2. *The 3–15 μm Spectral Range*

At the L' band and especially at the M band the host galaxy does not make a strong contribution. We used the L' nonstellar fractions derived by Alonso-Herrero et al. (1998) for the galaxies in common with our study. For the rest of the sample we estimated the nonstellar fractions at L' scaling the peak of the PSF surface brightness profile to that of the galaxy and assumed that the PSF integrated flux represents the unresolved component (see Alonso-Herrero et al. 1998 for more details). An alternative way of estimating the stellar contribution in L' can be done by using the typical colors $K-L'$ of a normal galaxy (Willner et al. 1984, and assuming a color transformation $L-L'=0.2$, Ward et al. 1982) and the stellar fractions at the K band. We find that the stellar contribution within a 3″ diameter aperture at L' are always less than 25% (except NGC 1052 for which we find a 65% of the total 3″ emission is stellar emission) and are in good agreement with the values estimated from the imaging data. The same procedure was applied to the M-band fluxes using the $K-M$ color of a normal galaxy (Rieke & Lebofsky 1978), and estimated that the stellar contribution at 4.8 μm within a 3″ diameter aperture is always less than 10%. This is supported by the compact appearance of all the observed sources at this wavelength. In Table 4, columns (5) and (6) we list the nonstellar fluxes at L' and M.

The small aperture L and M fluxes for the Seyfert 1 sample (compiled by Ward et al. 1987) are assumed to be all nonstellar in origin. The nonstellar fluxes along with the nonstellar fractions within a 3″ diameter aperture are given in Table 5. Note that the nonstellar 1.2–2.2 μm fluxes are not simultaneous with the 3.5–4.8 μm observations, which may add some uncertainty to the observed SEDs.

4. THE NONSTELLAR INFRARED EMISSION OF SEYFERT GALAXIES

Because the nonstellar contribution to the near-infrared continuum emission from Seyfert 1s usually dominates over the stellar emission, unlike the situation for Seyfert 2s (see e.g., Edelson & Malkan 1986; Kotilainen et al. 1992, and Alonso-Herrero et al. 1996), the SEDs of the nonstellar component is better defined in the Seyfert 1s. It is agreed that the infrared (up to 100 μm) SEDs of Seyfert 1s are well represented with a power law ($S_\nu \propto \nu^{-\alpha}$) with a canonical spectral index $\alpha \simeq 1$ (e.g., Edelson & Malkan 1986; Ward et al. 1987; Edelson, Malkan, & Rieke 1987; Granato & Danese 1994; Clavel et al. 2000). Similar spectral indices have been derived from the infrared SEDs of quasars (Edelson 1986; Neugebauer et al. 1987; Polletta et al. 2000; Haas et al. 2000). Fadda et al. (1998) have compiled infrared data from the literature for a sample of Seyfert 1s and Seyfert 2s, and found that the nonstellar SEDs of Seyfert 2s are always steeper than those of Seyfert 1s, in line with the finding that the 1–2.2 μm nonstellar fluxes of Seyfert 2s are significantly smaller than those of Seyfert 1s. However, the work of Fadda et al. (1998) and that of Murayama, Mouri, & Taniguchi (2000) suffer from a number of limitations when attempting to place constraints on the torus geometry based on the nonstellar infrared SEDs or colors. These

TABLE 5

NONSTELLAR FLUXES AND NONSTELLAR CONTRIBUTION WITHIN A 3″ DIAMETER APERTURE FOR THE SEYFERT 1 SAMPLE

Galaxy (1)	f(F110W) (mJy) (2)	f(F160W) (mJy) (3)	f(F222M) (mJy) (4)	$f(L)$ (mJy) (5)	$f(M)$ (mJy) (6)	J (percent) (7)	H (percent) (8)	K (percent) (9)
NGC 3227.....	...	10.6	22.6	78.3 ± 4.4	72 ± 27	...	21	32
NGC 4151.....	69.0	103.6	177.5	325 ± 10	449 ± 34	82	81	77
NGC 5548.....	...	15.0	31.6	98.6 ± 3.7	100 ± 21	...	57	59
NGC 7469.....	16.2	39.0	67.8	159 ± 5	259 ± 33	45	57	63
IC 4329A	...	49.9	101.8	210 ± 5	170 ± 20	...	71	75

NOTE.—The L and M fluxes are from Ward et al. (1987) and are assumed to be all nonstellar in origin.

works make use of nonsimultaneous observations, observations from different sources, uncertain nonstellar fluxes, and relatively large aperture N- and Q-band or *IRAS* fluxes, which may be contaminated by other contributions. Moreover, in order to understand the nature of the nonstellar SEDs of Seyfert 2 galaxies and in turn to constrain the torus geometry and derive the infrared extinctions to the central regions and their relation with the hard X-ray absorption columns, one cannot average the nonstellar SEDs of Seyfert 2s (or Seyfert 1s).

An additional problem often present in past statistical studies of SEDs is the grouping of galaxies into the Seyfert 1 and Seyfert 2 categories. A galaxy may be classified as a Seyfert 2 when it is observed in the optical (that is, no broad lines), but it may still show broad lines in the infrared, where the extinction is greatly reduced (see, for instance, Ruiz, Rieke, & Schmidt 1994; Goodrich, Veilleux, & Hill 1994; Veilleux, Goodrich, & Hill 1997). If using the latter observations, one would classify it as a Seyfert 1.8 or Seyfert 1.9. A better approach to the understanding of the infrared SED of Seyfert galaxies is to study each galaxy separately and determine whether a single torus geometry is able to fit most of the galaxies. Although in our study we do not claim a complete or unbiased sample of Seyfert 1s and 2s, because we have estimated accurate nonstellar SEDs we can compare these with current torus models and see whether there is a general agreement across the range of properties present in this sample. We will make use of Efstathiou & Rowan-Robinson (1995) models and discuss other models available in the literature. In addition to the galaxies presented in this work, we will fit the nonstellar infrared SED of NGC 3281 (nonstellar fluxes from Simpson 1998).

4.1. *The Efstathiou & Rowan-Robinson (1995) Models*

For our analysis we consider the tapered disk model of Efstathiou & Rowan-Robinson (1995). In this geometry, the height of the disk increases with the radial distance, but it tapers off to a constant height in the outer part. We will use a simple torus model (coneless) and a composite model with a torus and an optically thin cone. The latter model gave a better fit to the near-infrared emission in NGC 1068 (Efstathiou et al. 1995). The reasons for adding the optically thin component rather than using a simple torus model to fit the SED of NGC 1068 were twofold. First, this additional optically thin cone component increases the continuum around 3–5 μm, a condition necessary to fit the almost flat (in vf_v) observed SEDs of Seyfert 1s (see also below). This problem seems to affect all the current torus models (e.g., Pier & Krolik 1993; Granato & Danese 1994; and the model used here). Second, the simple torus model predicts strong absorption features at 9.7 μm for Seyfert 2s, which are not usually observed (Roche et al. 1991). See also the discussion in Efstathiou et al. (1995).

The model assumes a maximum dust temperature (dust sublimation temperature) of $T = 900$ K and the following parameters: $r_1/r_2 = 0.01$ (ratio of the inner and outer radii), $h/r_2 = 0.1$ (ratio of the height scale and the outer radius) and equatorial UV optical depth of $\tau_{UV} = 1200$, with a half-opening angle of the toroidal cone of $\theta_c = 30°$. We will also explore for comparison purposes another coneless model with a dust sublimation temperature of $T = 1500$ K.

A beaming factor was introduced by Efstathiou et al. (1995), basically to boost the near-infrared flux, as the inclusion of conical dust by itself did not provide sufficient emission in this spectral range. The beaming factor is defined as the ratio of the radiation intensity emitted by the continuum source toward the optically thin cone with respect to that directed toward the torus,

$$f_b = \frac{S_\nu(\theta < \theta_c)}{S_\nu(\theta \geq \theta_c)}, \quad (1)$$

where θ_c is the semi-opening angle of the torus, and θ is the angle measured from the pole. The beaming factor for this model ($f_b = 6$).

The viewing angles with $\theta_v = 0°$ polar view, and $\theta_v = 90°$ equatorial view (note that in Efstathiou & Rowan-Robinson 1995 models the authors measure the angles from the equator), UV optical depth, and corresponding visual extinctions of the coneless and cone torus model outputs are given in Table 6.

TABLE 6

VIEWING ANGLES, UV OPTICAL DEPTHS, AND EQUIVALENT VISUAL EXTINCTIONS FOR THE MODELS

θ_v (deg)	τ_{UV} (mag)	A_V (mag)
90	1200	221
84	1197	221
79	1018	188
73	914	169
64	812	150
50	700	129
44	658	121
40	620	114
36	558	103
30	263	49
30	50 (24)	9 (4)
25	2.5 (0)	0.5 (0)
20	2.5 (0)	0.5 (0)
10	2.5 (0)	0.5 (0)
0	2.5 (0)	0.5 (0)

NOTE.—In cols. (2) and (3) in parentheses are the values for the $T = 1500$ K model.

4.2. *SED Fitting*

The first step was to scale the outputs from the model to the observed SEDs in vf_v. The SED fitting was performed by minimizing the χ^2 function of the models and the observations for the varying viewing angles to the AGN and normalizations at different wavelengths, taking into account the errors due to the determination of the nonstellar fluxes and the photometric uncertainties. Note that we have not attempted to fit NGC 2992 or NGC 4968 because there are only four points for their SEDs. In Table 7 we list the best-fitting models (at 1 σ level confidence) for the SEDs, where n is the number of points in the SED, χ^2/ν is χ^2 per degree of freedom, θ_v is the best-fitting viewing angle (or range of angles), and the corresponding models.

In Figures 1–15 we present the observed SEDs ($\log vf_v$ in units of ergs per square centimeter per second) for the sample of Seyferts along with the best-fitting model scaled to the observed SED. The model outputs are plotted for the viewing angles given in Table 6 ($\theta_v = 0°$ is the top line, and θ_v increases to the bottom). The abrupt transition seen in the model output at viewing angle $\theta_v = 30°$ is due to the

TABLE 7

INFRARED NONSTELLAR SED MODELING

Galaxy	n	χ^2/ν	θ_v (deg)	Model
NGC 1068	7	1.0–1.6	40	Cone, $T = 900$ K, and no cone, $T = 1500$ K
NGC 3227	7	1.0	30	No cone, $T = 900$ K
NGC 3281	6	1.8–2.2	40	Cone and no cone, $T = 900$ K
NGC 4151	8	0.8	10	Cone, $T = 900$ K
NGC 5252	8	1.6	30	Cone, $T = 900$ K
NGC 5506	7	1.3	30	No cone, $T = 1500$ K
NGC 5548	7	0.9–1.0	10–30	Cone, $T = 900$ K, and no cone, $T = 1500$ K
NGC 7172	6	0.7–1.6	40	Cone, $T = 900$ K, and no cone, $T = 1500$ K
NGC 7469	9	1.1	0–30	Cone, $T = 900$ K, and no cone, $T = 1500$ K
Mrk 1	6	1.2	40–64	Cone and no cone, $T = 900$ K
Mrk 348	7	0.4–1.0	36–44	All
Mrk 533	7	1.5	30–36	Cone and no cone, $T = 900$ K
Mrk 573	6	0.4–0.8	36–50	Cone and no cone, $T = 900$ K
MCG −5-23-16.....	5	0.7–0.8	30–36	Cone and no cone, $T = 900$ K
IC 4329A	6	1.4	10	Cone, $T = 900$ K

NOTE.—χ^2/ν is χ^2 per degree of freedom, where $\nu = n-2$ and n is number of points for the SED.

assumed beaming factor. Using a beaming factor varying smoothly with θ would avoid the abrupt transition between those viewing angles.

As can be seen from Table 7 and Figures 1–15, the cone model provides good fits to the observed SEDs except in the cases of some intermediate SEDs (the SEDs of NGC 3227 and NGC 5506). The reason why the cone model fails to reproduce these intermediate SEDs is because of the abrupt transition produced for the assumed form of the beaming factor. If the beaming factor is decreased, then the cone model produces an acceptable fit to the SEDs of these galaxies, which is statistically indistinguishable from the coneless model. In some cases we find from our SED fitting that both the cone and coneless models produce indistinguishable fits at the 1 σ confidence level.

Despite the fact that we do not find compelling evidence to favor either the coneless or the cone model alone, we find that the viewing angle to the central source is very well constrained by the modeling of the SEDs. We find that none of the galaxies (not even the hard X-ray Compton-thick galaxies) in our sample show viewing angles greater than 64°, with most of the obscured Seyferts displaying values of between 30° and 40°. This does not mean that there are no Seyfert galaxies with $\theta_v > 65°$. First, the values for the fitted viewing angles will depend on the assumed geometry for the torus model (mainly, the equatorial optical depth and the beaming factor). Second, the shapes of the SEDs for viewing angles above 65° become almost parallel, with the added complication that the fitted viewing angle is very sensitive near-infrared nonstellar estimates. Finally, we stress that our sample is not complete or unbiased in the sense that we are most likely not including very obscured objects.

All the Seyfert 1s (see also Granato et al. 1997) except NGC 3227 show relatively flat SEDs implying viewing angles in the range $\theta_v = 0°$–30°—almost a face-on view. The coneless torus model does not account for the bright 1–5 μm emission present in NGC 4151 and IC 4329A. Other models also invoke additional near-infrared components in order to explain the SED of NGC 1068. Granato et al. (1997) assumed a model similar to the "anisotropic spheres" of Efstathiou & Rowan-Robinson (1995), whereas Pier & Krolik (1993) used a hot component made up of clouds inside the inner radius of the torus.

As expected, the Seyfert 2 galaxies show SEDs with different shapes well explained with the varying viewing angle to the central source. For example, NGC 5252 and NGC 5506 (both classified as Seyfert 1.9) appear to be seen at a viewing angle similar to that NGC 3227 (classified as a Seyfert 1.5). For the particular model assumed here it would be $\theta_v = 30°$. The similarity between the SEDs of NGC 5506, NGC 5252, and NGC 3227 is also supported by the detection in NGC 5506 and NGC 5252 of a broad line component in the infrared hydrogen recombination line Paβ (Rix et al. 1990; Blanco, Ward, & Wright 1990; and Ruiz et al. 1994, respectively). Veilleux et al. (1997), however, argued against the presence of such broad component in NGC 5506. Both galaxies also show relatively low hydrogen column densities derived from hard X-ray observations ($N_{\rm H} = 4.3$ and 3.4×10^{22} cm $^{-2}$ for NGC 5252 and NGC 5506, respectively, Bassani et al. 1999; equivalent to an optical extinction of $A_V \simeq 22$ and 17 mag for the standard gas-to-dust conversion factor). NGC 5506, NGC 5252, and NGC 3227 appear as good examples of why averaging properties of type 1 and type 2 objects may result in a loss of information.

The rest of the Seyfert 2s are viewed at angles $\theta_v \geq 30°$ (NGC 1068, NGC 3281, NGC 7172, Mrk 348, Mrk 533, and MCG −5-23-16). Of these galaxies Mrk 348, Mrk 533, and MCG −5-23-16 show broad components in infrared hydrogen recombination lines (Ruiz et al. 1994 for the first two and Veilleux et al. 1997 for MCG −5-23-16). Note however, that Veilleux et al. (1997) disputed the finding of broad lines in Mrk 533. The optical extinctions derived from hard X-ray observations (taken from Bassani et al. 1999) vary from moderate (MCG −5-23-16, $A_V \simeq 8$ mag), intermediate (NGC 7172 $A_V \simeq 60$ mag and NGC 3281 $A_V \simeq 400$ mag) to Compton-thick galaxies (NGC 1068 and Mrk 533). The most obscured SEDs in terms of the fitted viewing angles are Mrk 1 and Mrk 573. Neither galaxy shows broad infrared hydrogen recombination lines (Veilleux et al. 1997).

We find a tendency for the galaxies in our sample to have lower fitted extinctions from the SED modeling than those derived from hard X-ray hydrogen column densities for those galaxies with relatively high values of $N_{\rm H}$. The particular values of the extinctions derived from fitting the SEDs depend on the assumed equatorial UV optical depth. As

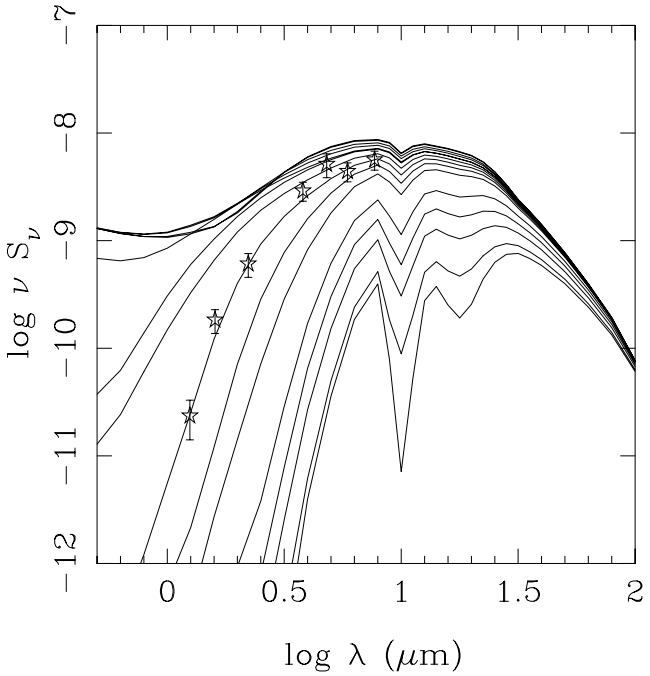

FIG. 1.—Observed SED and best-fitting model ($T = 1500$ K, no cone) for NGC 1068. The viewing angles (θ_v) for the model outputs increase from top to bottom.

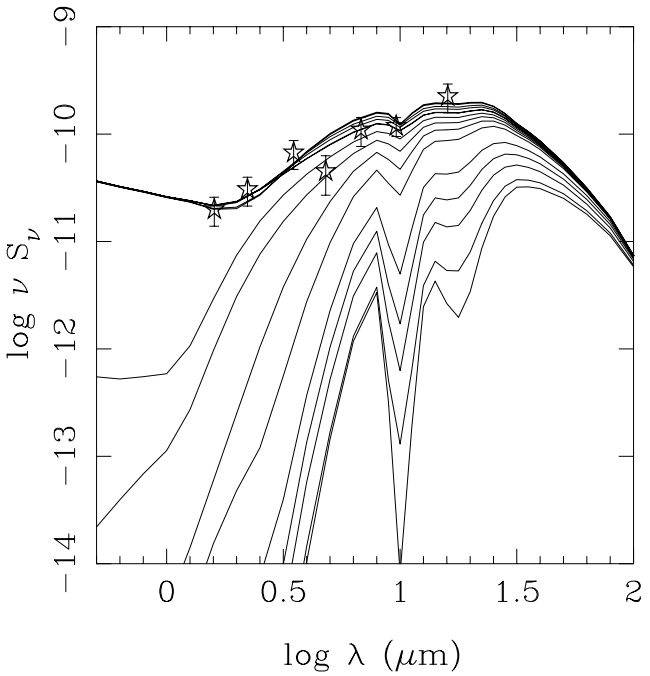

FIG. 2.—Same as Fig. 1, but for NGC 3227, model $T = 900$ K, no cone

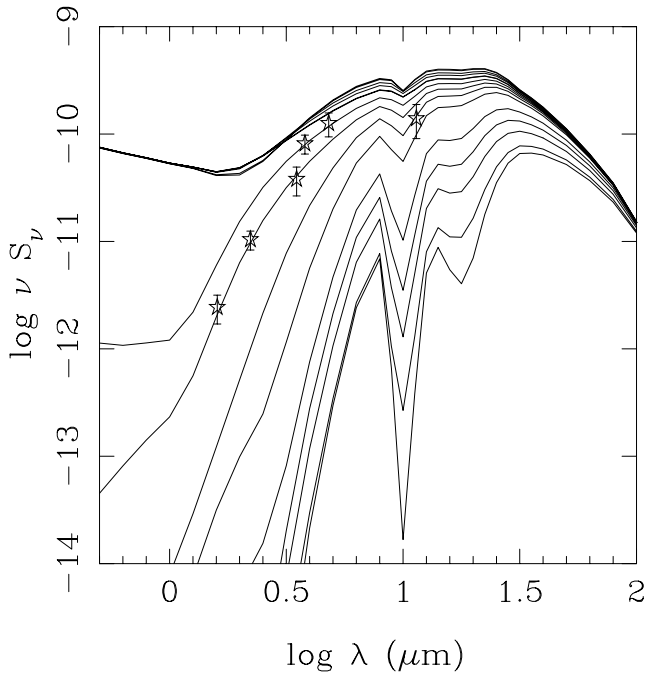

FIG. 3.—Same as Fig. 1, but for NGC 3281, model $T = 900$ K, no cone

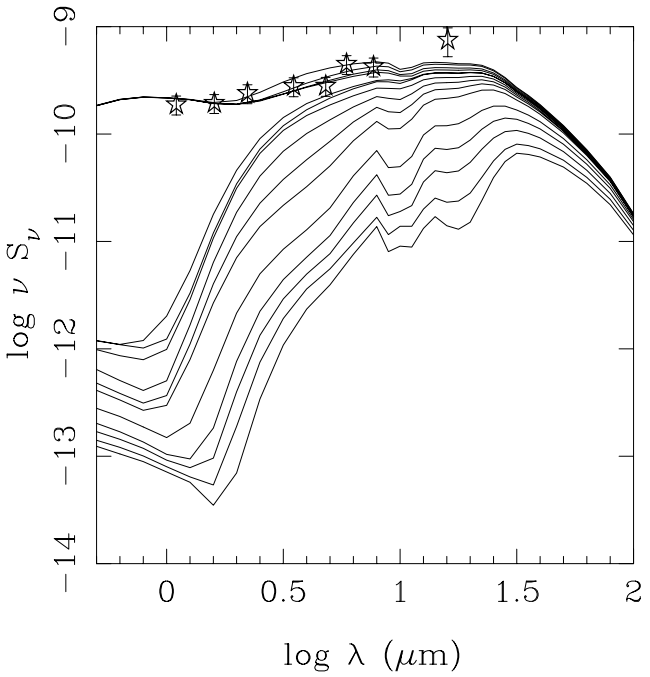

FIG. 4.—Same as Fig. 1, but for NGC 4151, model $T = 900$ K, cone

discussed in Efstathiou & Rowan-Robinson (1995) in order to reproduce the high extinction needed for Compton thick objects, it would be necessary to increase the value of τ_{UV} up to 4000 mag. This would cause the models to produce a very deep 10 μm absorption feature. The main difficulty in tori with optical depths of the order of a few thousands, however, is that the SEDs become too narrow as the temperature drops more steeply with radius. This is evident in the models of Pier & Krolik (1993), and it is basically the reason why the "optically thin dust" in their model for NGC 1068 is cooler than ours. But even if we were to assume a much higher equatorial optical depth, the infrared SEDs of two Compton thick galaxies in our sample (NGC 1068 and Mrk 533) are well reproduced with relatively modest extinctions that could not possibly be as elevated as those inferred from hard X-ray column densities. The rela-

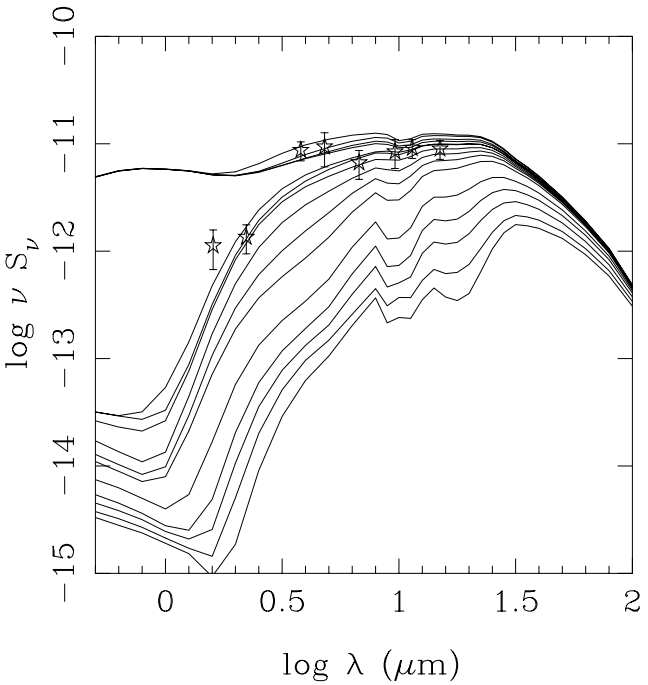

FIG. 5.—Same as Fig. 1, but for NGC 5252, model $T = 900$ K, cone

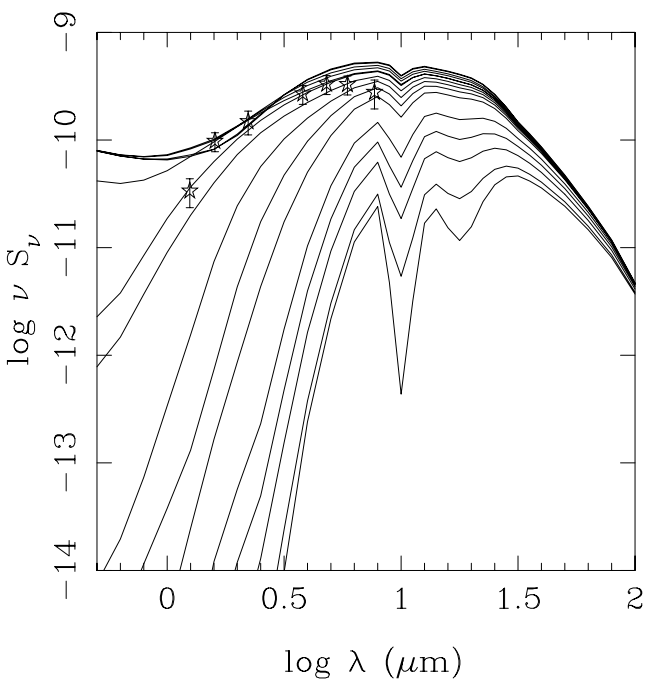

FIG. 6.—Same as Fig. 1, but for NGC 5506, model $T = 1500$ K, no cone.

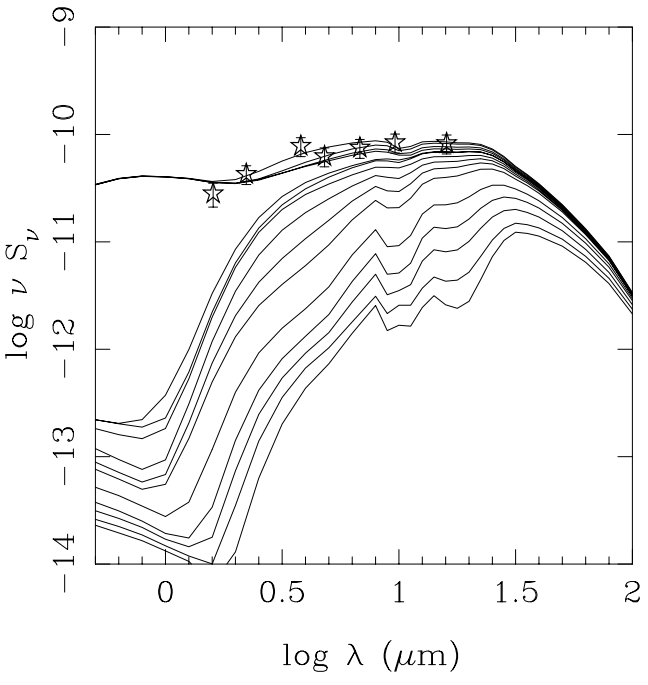

FIG. 7.—Same as Fig. 1, but for NGC 5548, model $T = 900$ K, cone

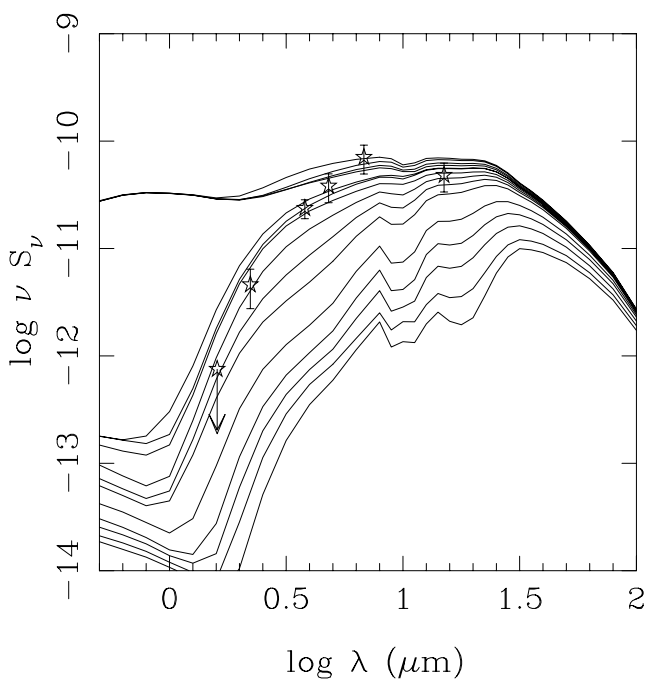

FIG. 8.—Same as Fig. 1, but for NGC 7172, model $T = 900$ K, cone

tively low values of the extinction needed for NGC 1068 were already noted in previous works (e.g., Efstathiou et al. 1995; Granato et al. 1997). We interpret the differing hard X-ray and infrared extinctions in the context of the torus + cone model. Most of the near-infrared emission seems to originate in the extended cone configuration which suffers less extinction than radiation emitted much closer to the active galactic nucleus (e.g., the hard X-rays).

4.3. *Nonstellar Color- Color Diagrams*

A number of works have attempted to use near-infrared to mid-infrared colors or flux ratios to constrain the obscuring torus geometry, to derive viewing angles to the torus, or to simply quantify the different observed properties between type 1 and type 2 Seyferts. For instance, Pier & Krolik (1993) used the $L-N$ colors for Seyfert galaxies to constrain the ratio a/h (that is, the ratio of the inner radius of

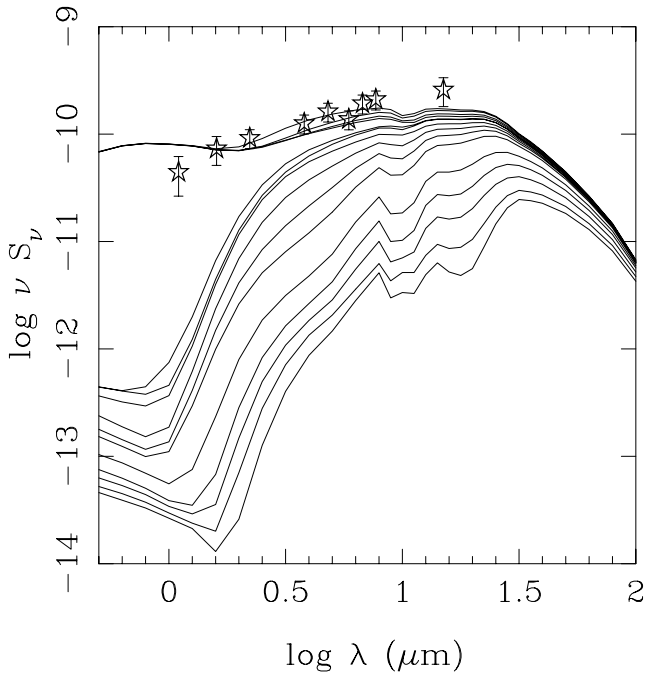

FIG. 9*a*

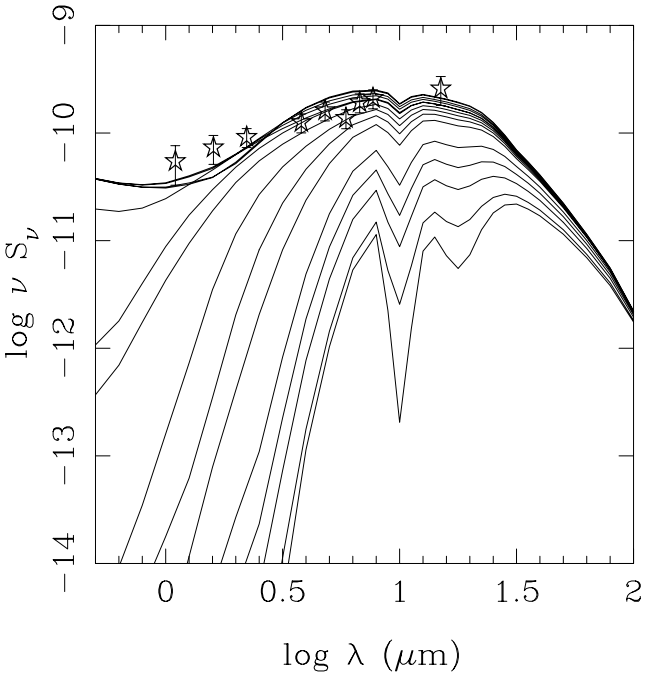

FIG. 9*b*

FIG. 9.—Same as Fig. 1, but for NGC 7469. (*a*) model $T = 900$ K, cone. (*b*) Model $T = 1500$ K, no cone.

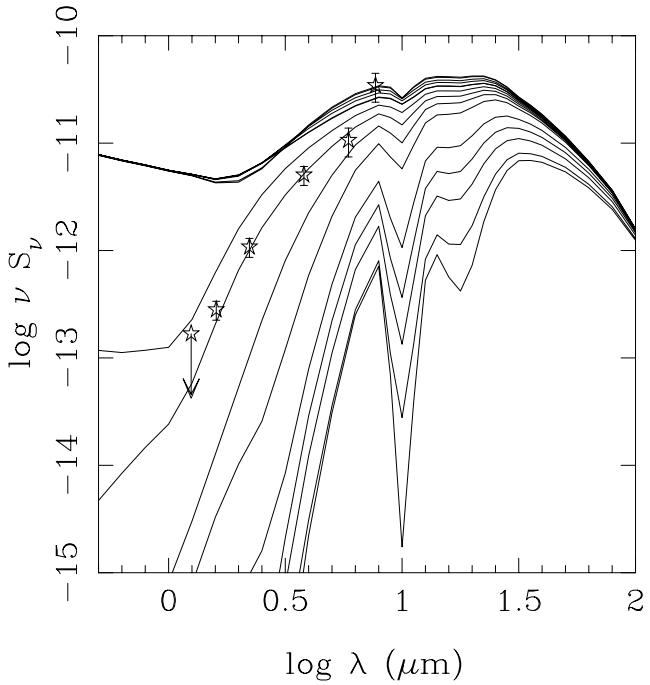

FIG. 10.—Same as Fig. 1, but for Mrk 1, model $T = 900$ K, no cone

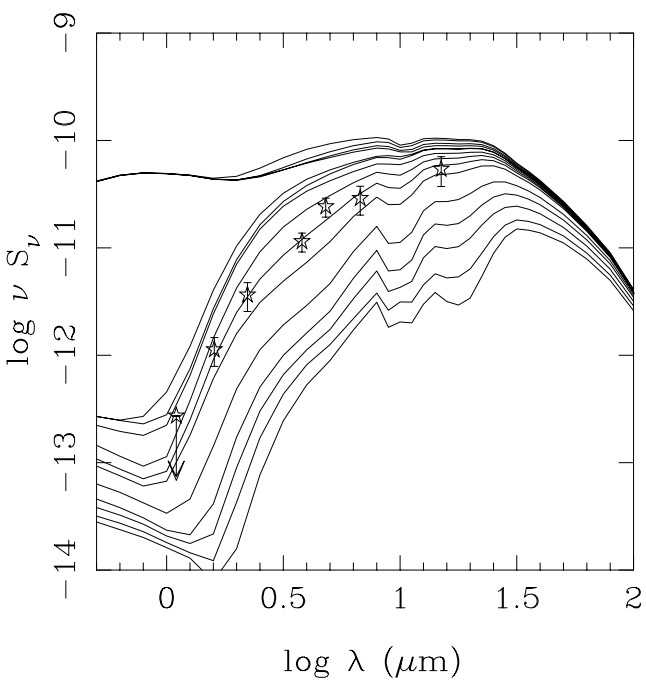

FIG. 11.—Same as Fig. 1, but for Mrk 348, model $T = 900$ K, cone

the torus to its thickness and therefore the opening angle of the torus), but failed to reproduce the $L-N$ colors of Seyfert 2s, as well as the flat SEDs of Seyfert 1s and PG quasars. Murayama et al. (2000) have used Pier & Krolik (1993) models and the ratio of the L (3.5 μm) and IRAS 25 μm fluxes to derive torus properties such as the opening angle and the critical viewing angle for which the broad-line region (BLR) is visible. Fadda et al. (1998) compared the average of number of near-infrared and mid-infrared colors for Seyfert 1s and 2s with predictions of a wide series of models. These studies, as mentioned above, may suffer from unquantified large aperture effects in the mid-infrared where the underlying galaxy and/or star formation may make a significant contribution.

We explore nonstellar color-color diagrams involving observations with $\lambda < 5$ μm for which we are certain about the nonstellar contribution. Because of the large apertures employed by the ISO instruments, there may be a signifi-

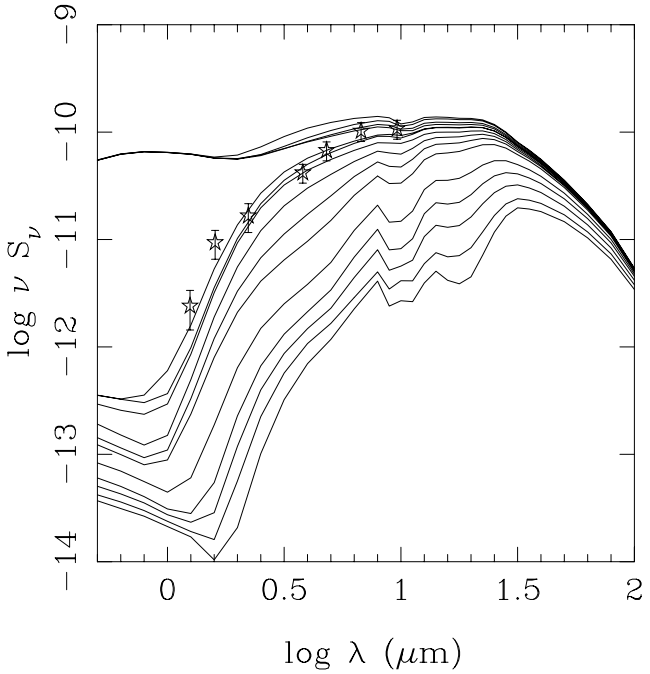

FIG. 12.—Same as Fig. 1, but for Mrk 533, model $T = 900$ K, cone

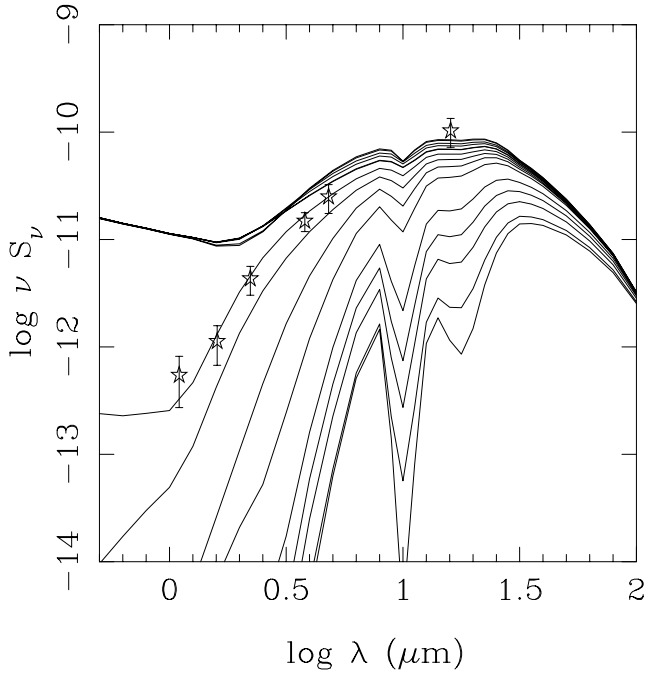

FIG. 13.—Same as Fig. 1, but for Mrk 573, model $T = 900$ K, no cone

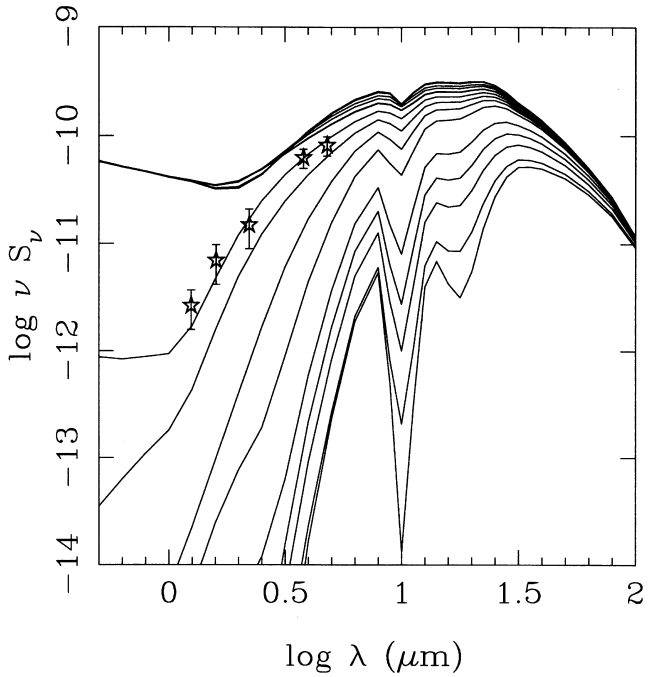

FIG. 14.—Same as Fig. 1, but for MCG−5-23-16, model $T = 900$ K, no cone.

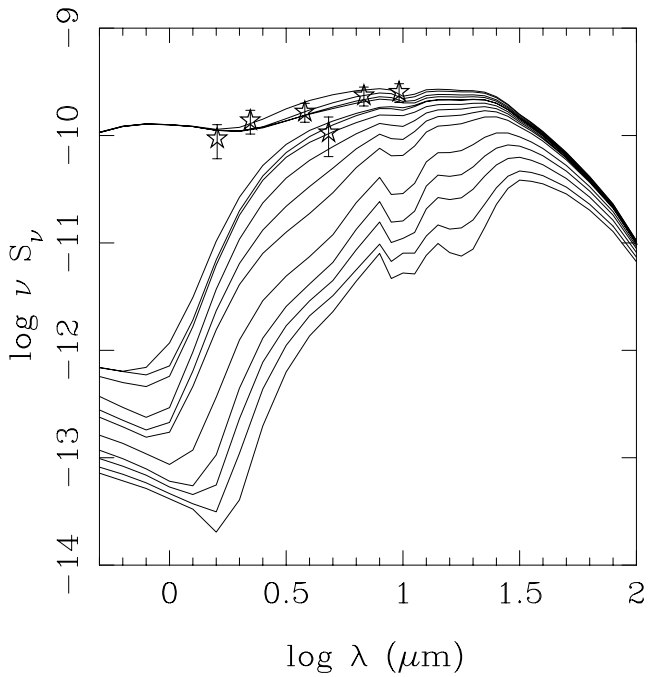

FIG. 15.—Same as Fig. 1, but for IC 4329A, model $T = 900$ K, cone

cant stellar contribution. In Figure 16 we present nonstellar color-color diagrams: $L'-M$ versus $H-M$ [vf_ν(3.8 μm)/vf_ν(4.8 μm) vs. vf_ν(1.6 μm)/vf_ν(4.8 μm), *top panels*] and $L'-M$ versus $H-L'$ [vf_ν(3.8 μm)/vf_ν(4.8 μm) vs. vf_ν(1.6 μm)/vf_ν(3.8 μm), *bottom panels*]. The left panels show the sample of Seyfert galaxies. For the Seyfert 1s in Table 5 the 3.8 μm fluxes have been interpolated using the 3.5 and 4.8 μm fluxes. The errors at 1.6 μm account for the uncertainty associated with the nonstellar flux determination, whereas the errors at 3.8 and 4.8 μm are due to the photometry and sky subtraction uncertainties. We have divided the sample of Seyferts into galaxies with fitted viewing angles $\theta_v \leq 30°$ and $\theta_v \geq 30°$. NGC 2992 and NGC 4968 are plotted with the symbol for unknown θ_v since they were not fitted in the preceding section. In the right panels we show the outputs from the torus + cone model, and the coneless torus models with dust sublimation temperatures $T = 900$, 1500 K. The crosses on the lines are the different viewing angles

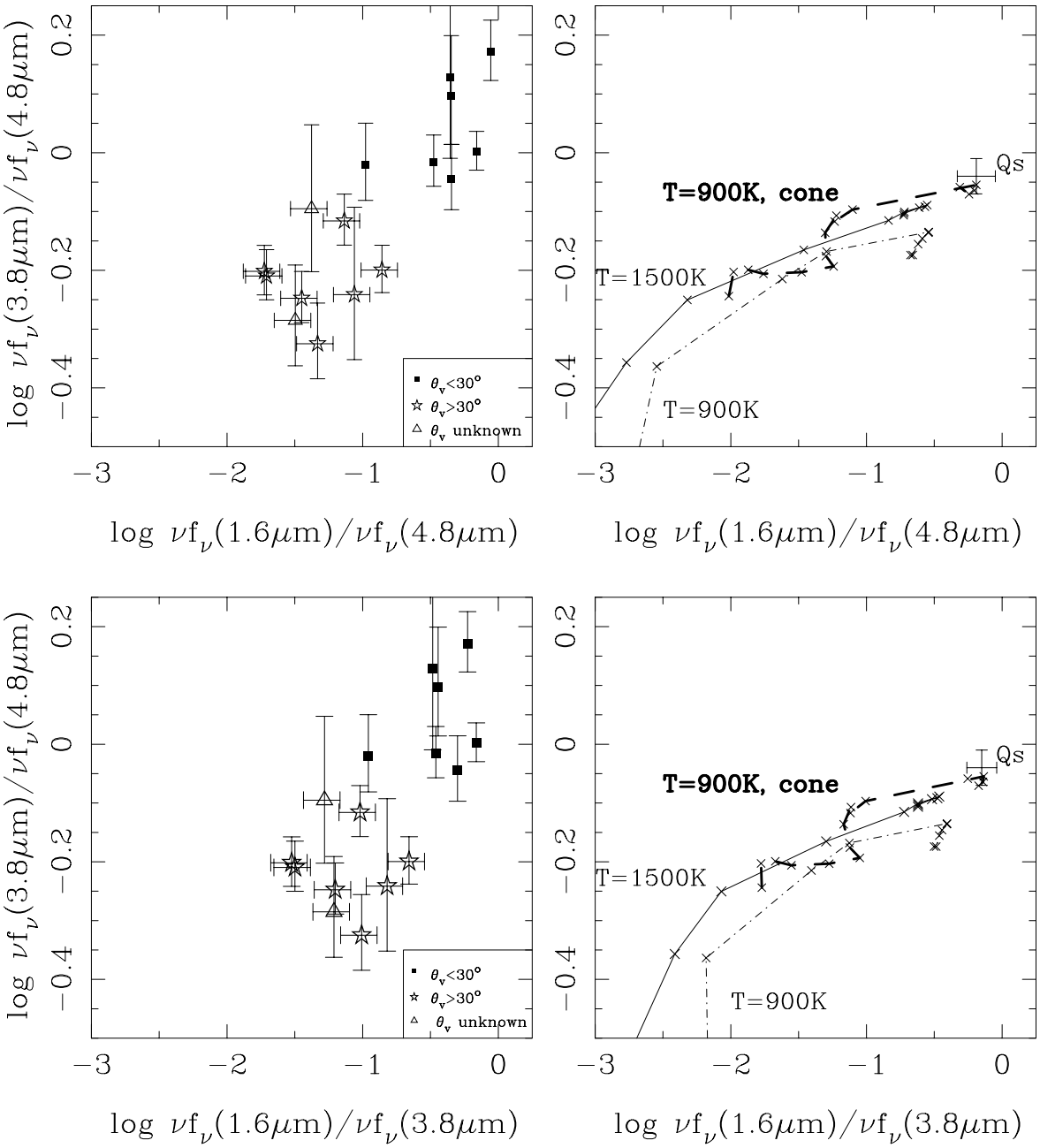

FIG. 16.—Nonstellar near-infrared color-color maps. The left panels show the data for the sample of Seyfert galaxies, divided into galaxies with viewing angles $\theta_v \leq 30°$ and $\theta_v \geq 30°$. The right panels show the outputs from Efstathiou et al. (1995) models for the torus + cone component model (*thick lines*), and for the torus alone (*coneless*) model with two dust sublimation temperatures, $T = 900$ K (*dot-dash lines*) and $T = 1500$ K (*solid lines*). The crosses on the lines indicate the viewing angles (see Table 6), which increase to the left. We also show the average position of low redshift PG quasars (see text).

(*increasing to the left*). We also show the average position of nearby PG quasars using a near-mid infrared spectral index of $\alpha = 1.4 \pm 0.13$ (Neugebauer et al. 1987).

The effect of adding the cone component is readily seen from this figure. The cone model is able to reproduce the *bluer* (that is, flatter SEDs) $H-L'$, $H-M$, and $L'-M$ colors of the average PG quasar, and the Seyferts with $\theta_v \leq 30°$. Note that the three Seyfert 1s located in the upper right corner (NGC 3227, NGC 4151, and IC 4329A) have anomalous M-band fluxes (too low) as seen from the SEDs in Figures 1–15. In addition, the coneless models produce much redder colors for large values of the viewing angles, but these are not observed in our sample.

These two color-color diagrams provide a good means to separate Seyfert 2 galaxies with modest obscuration, A_V up to $\simeq 20$ mag from hard X-ray observations (e.g., NGC 5252, NGC 5506, and MCG −5-23-16, NGC 2992), from those with high obscuration. The two galaxies whose SEDs were not fitted in the preceding section also fit into these two categories. NGC 2992 displays a moderate absorption from hard X-ray observations, whereas NGC 4968 is a Compton-thick galaxy (Bassani et al. 1999). There appears to be a transition at around $\log \nu f_\nu(3.8\ \mu\text{m})/\nu f_\nu(4.8\ \mu\text{m}) \simeq -0.15$. This may be interpreted as corresponding to a critical viewing angle for a relatively hard edge torus, above which the BLR becomes visible. This critical value is larger than

the opening angle. The separation between the two classes is not so well defined if the $\log \nu f_\nu(1.6\ \mu m)/\nu f_\nu(4.8\ \mu m)$ [or $\log \nu f_\nu(1.6\ \mu m)/\nu f_\nu(3.8\ \mu m)$] flux ratio is used instead, probably due to other effects such as foreground extinction still affecting the 1.6 μm fluxes (see Quillen et al. 2001b for a detailed discussion on this issue).

5. MID-INFRARED EMISSION OF AGN, AN INDICATOR OF THE AGN LUMINOSITY?

5.1. *The Mid-Infrared versus Hard X-Ray Correlations*

As mentioned in the introduction all torus models predict strong emission at mid-infrared wavelengths. Based on ISO observations of quasars it has been found that there is a good correlation between the infrared (3–40 μm) luminosities and other properties (blue luminosity, soft X-ray luminosities) and this is indicative that an important fraction of the mid-infrared energy is produced by dust heated by the AGN (Polletta et al. 2000; Haas et al. 2000). To test if this is the case for both Seyfert 1s and Seyfert 2s, it is necessary to have a good indicator of the AGN luminosity to which we can ratio the mid-infrared emission.

The hard X-ray (2–10 keV) emission of Seyfert galaxies is known to be a good indicator of the intrinsic luminosity of the AGN for those cases where it is transmitted through the torus, that is, in Compton thin galaxies. Other proposed indicators of the AGN power of both Seyfert 1s and Seyfert 2s include the [O III] λ5007 luminosity (Mulchaey et al. 1994; Heckman 1995) or the nonthermal 1.45 GHz radio continuum (Heckman 1995). The [O III] luminosities may be affected by extinction, distribution of the gas in the parent galaxy, and star formation. Heckman (1995) found that the 10.6 μm emission of Seyfert 2s when ratioed to the nonthermal 1.4 GHz emission is 4 times smaller than that of Seyfert 1s, and this would suggest that even the mid-infrared emission of Seyfert 2s is anisotropic. However, caution is needed when interpreting Heckman's result; the radio emission of Seyfert galaxies may not be an isotropic property because of Doppler boosting of the core emission in Seyfert 1s. Because of the uncertainties associated with the use of the radio and [O III] luminosities as indicators of the AGN power, we will test the above assumption using hard X-ray measurements.

We use the M-band (4.8 μm) measurements presented in this work for Seyfert 2 galaxies and for other Seyferts (mainly Seyfert 1s compiled by Ward et al. 1987), the ISO 9.63 μm fluxes from Clavel et al. (2000), hard X-ray (2–10 keV) measurements (compiled by Mulchaey et al. 1994 and Alonso-Herrero et al. 1997, and references therein), and new measurements from Bassani et al. (1999). The hard X-ray fluxes of Seyfert 2s have been corrected for the intrinsic absorption.

In Figures 17 and 18 we plot the correlations in fluxes and luminosities (for $H_0 = 75$ km s^{-1} Mpc^{-1}) for the 4.8 and 9.63 μm measurements, respectively. Both figures provide good evidence that the 5–10 μm emission in AGNs is powered by the central source. Note that in these two diagrams only Seyfert 2 galaxies with relatively low attenuations for which the hard X-rays are transmitted (Compton thin, $N_H \leq 10^{24}$ cm^{-2}, or $A_V \lesssim 500$ mag) are plotted. A similar correlation has been found by Krabbe, Böker, & Maiolino (2000) using N-band (at 10.2 μm) imaging of a small sample of Seyfert galaxies. These two correlations between the hard X-ray and the mid-infrared luminosities are very much improved even for Seyfert 2 galaxies when compared with shorter wavelengths (2.2 and 3.5 μm, Alonso-Herrero et al. 1997).

We have performed a statistical analysis of the correlations (both in fluxes and luminosities) using the ASURV survival analysis program (Isobe & Feigelson 1990; LaValley, Isobe, & Feigelson 1992). The results are tabulated in Table 8. For the L-band versus hard X-ray correlations we have used the data for Seyfert 1s and 2s presented in Alonso-Herrero et al. (1997). In this study we demonstrated

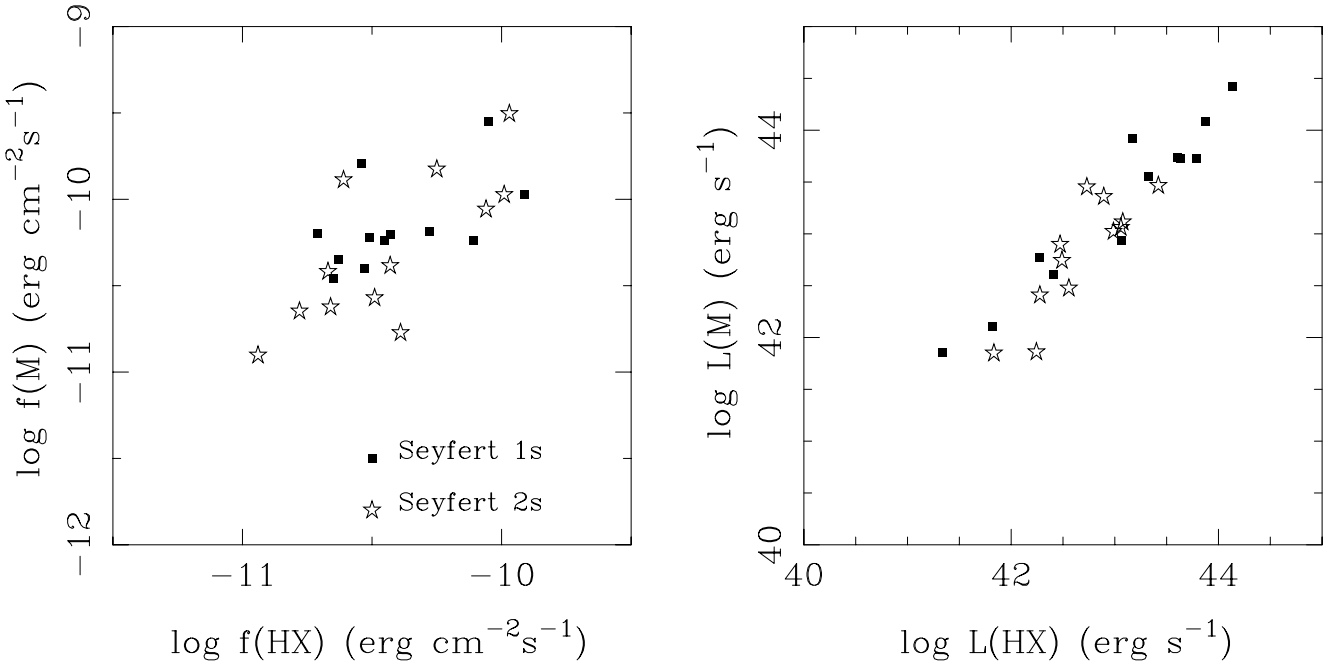

FIG. 17.—M-band versus hard X-ray (2–10 keV) correlations in flux (*left panel*) and luminosities (*right panel*)

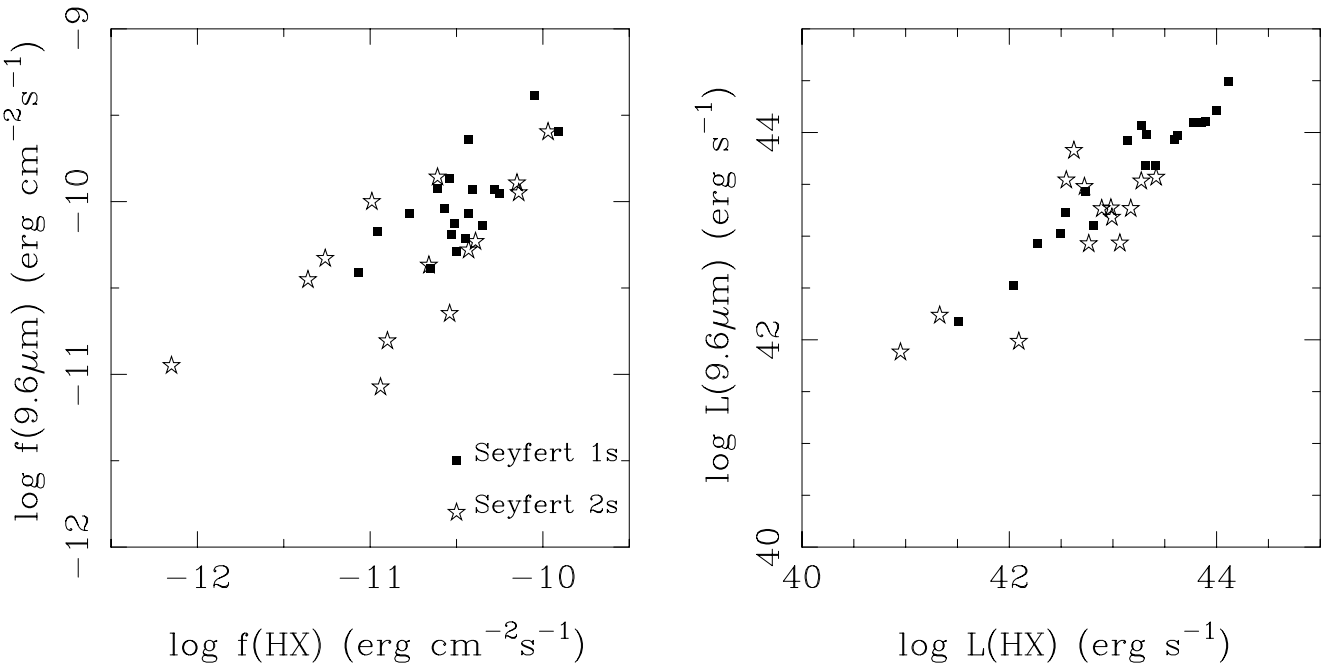

FIG. 18.—Same as Fig. 17, but with the ISO 9.63 μm fluxes and luminosities

that for some Compton-thin Seyfert 2 galaxies much of the L-band (3.5 μm) emission is attenuated, and this fact was used to estimate the extinctions to the AGN. The reason for the improved correlations in the mid-infrared (4.8 and 9.6 μm) is the reduced extinction as the wavelength increases. As we saw in § 4.2, in our sample there are no Seyfert galaxies with viewing angles $\theta_v > 64°$. This means that we should not expect extinctions higher than $A_V = 130$ mag or $A(4.8\ \mu\text{m}) \simeq 3$ mag (using Rieke & Lebofsky 1985 extinction law), which is in good agreement with the observed scatter in the 4.8 μm versus hard X-ray correlation.

As discussed in § 4.1, in the torus + cone model most of the near-infrared emission is produced in the optically thin cone. This component is located between the BLR and the NLR. The conical dust is more visible from all viewing angles, and it is probably illuminated by a stronger continuum (due to the beaming). This is confirmed by the findings of Bock et al. (1998) that NGC 1068 shows dust emission from the wall of the cavity, i.e., perpendicular to the axis of the torus and in an extended component ($\simeq$100 pc) coincident with the radio emission and ionization cone (Alloin et al. 2000). This naturally explains the good correlation between the 4.8 and 9.7 μm and the hard X-ray emissions.

TABLE 8

CORRELATION STATISTICS FOR SEYFERT 1S AND SEYFERT 2S

Correlation	Quantity	N	r_S	Probability
L-band vs. HX	Flux	33	0.26	1.4×10^{-1}
M-band vs. HX.....	Flux	24	0.61	3.3×10^{-3}
9.6 μm vs. HX	Flux	33	0.66	2.0×10^{-4}
L-band vs. HX	Lum	33	0.90	$<7 \times 10^{-6}$
M-band vs. HX.....	Lum	24	0.94	6.8×10^{-6}
9.6 μm vs. HX	Lum	33	0.90	6.7×10^{-7}

NOTE.—N is the number of objects in the sample, r_S is the Spearman correlation rank, and Probability is the probability that the correlation is not present.

Moreover, this may offer an explanation for the Compton optically thick Seyferts ($N_H > 10^{24}$ cm^{-2}) that are bright in the mid-infrared. The examples in our sample are NGC 1068, Mrk 533, and NGC 4968. This kind of objects are also present in the CfA sample (Quillen et al. 2001b). We conclude that the 5–10 μm emission in Seyfert galaxies is a good indicator of the AGN power.

5.2. *Mid-Infrared Counterparts of Highly Obscured X-Ray Galaxies*

The use of mid-infrared measurements as indicators of the AGN luminosity may have very important implications. Recent deep field surveys from Chandra have found a number of hard X-ray sources which are not identified optically (e.g., Mushotzky et al. 2000). These sources are candidates for the highly absorbed objects needed to account for the spectral index of the hard X-ray background (Setti & Woltjer 1989). Some of the X-ray identified sources require high levels of absorption to account for the flatness of their X-ray spectrum, suggesting that these sources might be opaque even at 10 μm. A recent comparison of faint SCUBA sources with Chandra sources found only one source in common (Fabian et al. 2000). However, in the preceding section we have shown that Compton-thick sources can be bright in the mid-infrared. If such sources are common then follow up deep surveys can search for mid-infrared counterparts to highly absorbed X-ray sources.

For the non-Compton thick sources ($N_H \leq 10^{24}$ cm^{-2}) the 5 μm luminosity is similar to that at 2–10 keV (Fig. 17). Mushotzsky et al. (2000) found 2000 and 300 sources per square degree with 2–10 keV fluxes greater than 2×10^{-15} and 10^{-14} ergs cm^{-2} s^{-1}, respectively. These sources would correspond to fluxes of 3 and 17μJy at rest wavelength of 5 μm. If the rest 10 and 20 μm luminosities are twice that of 5 μm flux, then we would expect 13 and 66 μJy at a rest wavelength of 10 μm and 26 and 130μJy at a rest wavelength of 20 μm for these sources.

The K-correction in the mid-infrared is likely to make the observed sources more difficult to detect since the spectrum is red out to ~ 30 μm. The obscured sources are most likely to be detected between ~ 15–90 μm where the rest wavelength 5–30 μm peak is redshifted into the observed wavelength range, though unobscured sources would suffer less from the K correction. Deep mid-IR surveys planned with SIRTF will go deep enough over large enough areas that mid-IR candidates to absorbed X-ray sources should be found. However we expect based on ISO surveys that in this wavelength region the number of counts from starbursts will dominate by at least an order of magnitude the counts from AGNs. If these sources are at a redshift of 2.0 then the X-ray luminosity of a source with hard X-ray fluxes 10^{-14} ergs cm^{-2} s^{-1} is only $\sim 10^{44}$ ergs s^{-1} (assuming $q_0 = 0.15$ and $H_0 = 75$) which implies that these sources might just be Seyferts. If they are L^* galaxies they would be difficult to detect in optical follow-up searches ($m_I > 26$).

6. SUMMARY AND CONCLUSIONS

We have presented 1–5 μm imaging for a sample of Seyfert 2 galaxies. The data have been complemented with existing *HST*/NICMOS (1–2.2 μm) and ISO (6–15 μm) observations of the Seyfert 2s, as well as a small comparison sample of Seyfert 1s. We have performed a very careful estimate of the nonstellar fluxes in the 1–5 μm range to construct nonstellar infrared SEDs. We fit the nonstellar infrared (up to 15 μm) SEDs with the Efstathiou & Rowan-Robinson (1995) code for tapered disks. We consider a simple torus model (coneless) and a composite model which includes a torus and an optically thin cone component. The latter model was found to fit well the SED of NGC 1068 (Efstathiou et al. 1995). From our analysis we find that:

1. The nonstellar infrared SEDs for the Seyfert galaxies in our sample display a variety of shapes, which can all be well fitted by either cone or coneless models. Although the model fits to the SEDs do not clearly favor the cone models, as claimed by Efstathiou et al. (1995), we nevertheless find that the viewing angle toward the central source is well constrained even in cases where the fits to the cone and coneless models are equally valid. For all the galaxies in our sample we find viewing angles $\theta_v \leq 64°$, with most of the obscured galaxies showing $\theta_v \simeq 40°$. The fitted viewing angles are however dependent on the assumed torus geometry.

2. The nonstellar $L'-M$ versus $H-L'$ and $H-M$ color-color diagrams provide a good means to separate those Seyfert 2s with moderate obscurations ($A_V \lesssim 20$ mag from hard X-ray observations) from those with high obscuration. The $L'-M$, $H-L'$, and $H-M$ colors of Seyfert 1s and Seyfert 2s with viewing angles of $\theta_v < 30°$ are better reproduced with the cone model.

3. The extinctions derived from the model fits to the SEDs tend to be less than those inferred from measurements of the hard X-ray attenuations. This can be understood if the material responsible for obscuration of the infrared continuum is in a different location from the gas column causing absorption of the X-rays.

4. There is a good correlation between 4.8 μm and ISO 9.7 μm and hard X-ray fluxes and luminosities for both Seyfert 1s and Compton thin ($N_H \leq 10^{24}$ cm^{-2}) Seyfert 2s. The improved correlations at 4.8 and 9.7 μm with respect to those at shorter wavelengths are explained in terms of the reduced extinction. Some Compton thick sources (e.g., NGC 1068 and Mrk 533) are bright infrared sources suggesting that the component responsible for the bulk of the infrared emission in Seyfert galaxies is more visible from all viewing angles than that responsible for the hard X-ray emission. We conclude that the mid-infrared emission in Seyfert galaxies can be used as a measure of the AGN luminosity. This has important implications for future mid-infrared searches of visually obscured objects which may make an important contribution to the hard X-ray background.

We are grateful to P. Martini for providing us with some of the NICMOS images used in this work prior to their publication. We also thank M. Ruiz for useful discussions. A. A.-H. was partially supported by the National Aeronautics and Space Administration on grant NAG 5-3042 through the University of Arizona. A. A.-H. thanks the Department of Physics and Astronomy, University of Leicester for their warm hospitality.

REFERENCES

Alexander, D. M., Efstathiou, A., Hough, J. H., Aitken, D. K., Lutz, D., Roche, P. F., & Sturm, E. 1999, MNRAS, 310, 78
Alloin, D., Pantin, E., Lagage, P. O., & Granato, G. L. 2000, A&A, 363, 926
Alonso-Herrero, A., Simpson, C., Ward, M. J., & Wilson, A. S. 1998, ApJ, 495, 196
Alonso-Herrero, A., Ward, M. J., & Kotilainen, J. K. 1996, MNRAS, 278, 902
———. 1997, MNRAS, 288, 977
Andreani, P., Franceschini, A., & Granato, G. 1999, MNRAS, 306, 161
Barvainis, R. 1987, ApJ, 320, 537
Bassani, L., Dadina, M., Maiolino, R., Salvati, M., Risaliti, G., Della Ceca, R., Matt, G., & Zamorani, G. 1999, ApJS, 121, 473
Blanco, P. R., Ward, M. J., & Wright, G. S. 1990, MNRAS, 242, P4
Bock, J. J., Marsh, K. A., Ressler, M. E., & Werner, M. W. 1998, ApJ, 504, L5
Clavel, J., et al. 2000, A&A, 357, 839
Danese, L., Zitelli, V., Granato, G. L., DeZotti, G., & Mandolesi, N. 1992, ApJ, 399, 38
Edelson, R. A. 1986, ApJ, 309, L69
Edelson, R. A., & Malkan, M. A. 1986, ApJ, 308, 59
Edelson, R. A., Malkan, M. A., & Rieke, G. H. 1987, ApJ, 321, 233
Efstathiou, A., Hough, J. H., & Young, S. 1995, MNRAS, 277, 1134
Efstathiou, A., & Rowan-Robinson, M. 1995, MNRAS, 273, 649
Elias, J. H., Frogel, J. A., Matthews, K., & Neugebauer, G. 1982, AJ, 87, 1029
Fabian, A. C., et al. 2000, MNRAS, 315, L8
Fadda, D., Giuricin, G., Granato, G. L., & Vecchies, D. 1998, ApJ, 496, 117
Goodrich, R. W., Veilleux, S., & Hill, G. J. 1994, ApJ, 422, 521
Granato, G. L., & Danese, L. 1994, MNRAS, 268, 235
Granato, G. L., Danese, L., & Franceschini, A. 1997, ApJ, 486, 147
Haas, M., Müller, S. A. H., Chini, R., Meisenheimer, K., Klaas, U., Lemke, D., Kreysa, E., & Camenzind, M. 2000, A&A, 354, 453
Heckman, T. M. 1995, ApJ, 446, 101
Isobe, T., & Feigelson, E. D. 1990, BAAS, 29, 917
Kotilainen, J. K., Ward, M. J., Boisson, C., DePoy, D. L., Smith, M. G., & Bryant, L. R. 1992, MNRAS, 256, 125
Krabbe, A., Böker, T., & Maiolino, R. 2000, ApJ, in press
Krist, J. E., Golimowski, D. A., Schroeder, D. J., & Henry, T. J. 1998, PASP, 110, 1046
LaValley, M., Isobe, T., & Feigelson, E. D. 1992, in ASP Conf. Ser. 25, Astronomical Data Analysis Software and Systems I, ed. D. M. Worrall, C. Biemesderfer, & J. Barnes (San Francisco: ASP), 245
Malkan, M. A., Gorjian, V., & Tam, R. 1998, ApJS, 117, 25
McAlary, C. W., & Rieke, G. H. 1988, ApJ, 333, 1
McLeod, B. A. 1997, in The 1997 *HST* Calibration Workshop, ed. S. Casertano, R. Jedrzejewski, C. D. Keyes, & M. Stevens (Baltimore: STScI), 281
Mulchaey, J. S., Koratkar, A., Ward, M. J., Wilson, A. S., Whittle, M., Antonucci, R. R. J., Kinney, A. L., & Hurt, T. 1994, ApJ, 436, 586
Murayama, T., Mouri, H., & Taniguchi, Y. 2000, ApJ, 528, 179

Mushotzky, R. F., Cowie, L. L., Barger, A. J., & Arnaud, K. A. 2000, Nature, 404, 459
Neugebauer, G., Green, R. F., Matthews, K., Schmidt, M., Soifer, B. T., & Bennett, J. 1987, ApJS, 63, 615
Pérez García, A. M. & Rodríguez Espinosa, J. M. 2000 (astro-ph/0003349)
Pier, E. A., & Krolik, J. H. 1992, ApJ, 401, 99
———. 1993, ApJ, 418, 673
Polletta, M., Courvoisier, T. J.-L., Hooper, E. J., & Wilkes, B. J. 2000, A&A, 362, 75
Quillen, A. C., McDonald, C., Alonso-Herrero, A., Lee, A., Shaked, S., Rieke, M. J., & Rieke, G. H. 2001a, ApJ, 547, 129
Quillen, A. C., Shaked, S., Alonso-Herrero, A., McDonald, C., Lee, A., Rieke, M. J., & Rieke, G. H. 2000, ApJ, 532, L17
Quillen, A. C., Alonso-Herrero, A., et al., 2001b, in preparation
Rieke, G. H. 1978, ApJ, 226, 550
Rieke, G. H., & Lebofsky, M. J. 1978, ApJ, 220, L37
———. 1985, ApJ, 288, 618
Rieke, G. H., & Low, F. J. 1975, ApJ, 199, L13
Rigopoulou, D., Spoon, H. W. W., Genzel, R., Lutz, D., Moorwood, A. F. M., & Tran, Q. D. 1999, AJ, 118, 2625
Rix, H.-W., Carlenton, N. P., Rieke, G., & Rieke, M. 1990, ApJ, 363, 480
Roche, P., Aitken, D. K., Smith, C. H., & Ward, M. J. 1991, MNRAS, 248, 606
Ruiz, M., Efstathiou, A., Alexander, D., & Hough, J. 2001, MNRAS, in press
Ruiz, M., Rieke, G. H., Schmidt, G. D. 1994, ApJ, 423, 608
Sanders, D. B., Phinney, E. S., Neugebauer, G., Soifer, B. T., & Matthews, K. 1989, ApJ, 347, 29
Setti, G., & Woltjer, L. 1989, A&A, 224, L21
Simpson, C. 1998, ApJ, 509, 653
Veilleux, S., Goodrich, R. W., & Hill, G. J. 1997, ApJ, 477, 631
Ward, M. J., Allen, D. A., Wilson, A. S., Smith, M. G., & Wright, A. E. 1982, MNRAS, 199, 953
Ward, M., Elvis, M., Fabbiano, G., Carleton, N. P., Willner, S. P. & Lawrence, A. 1987, ApJ, 315, 74
Willner, S. P., Fabbiano, G., Elvis, M., Ward, M., Longmore, A., & Lawrence, A. 1984, PASP, 96, 143
Zitelli, V., Granato, G. L., Mandolesi, N., Wade, R., & Danese, L. 1993, ApJS, 84, 185